Manipulating sublattice distortion induced by Mn^{2+} doping for boosting the emission characteristics of self-trapped exciton in Cs_4SnBr_6

Zhenxu Lin,[a] Anyang Wang,[c] Rui Huang,[b] Haixia Wu,[b] Jie Song,[b] Zewen Lin,[b] Dejian Hou,[b] Zhaofu Zhang,[d] Yuzheng Guo†, [c] and Sheng Lan‡,[a]*

a. Guangdong Provincial Key Laboratory of Nanophotonic Functional Materials and Devices, School of Information and Optoelectronic Science and Engineering, South China Normal University, Guangzhou 510006, China

b. School of Material Science and Engineering, Hanshan Normal University, Chaozhou 521041, China

c. School of Electrical Engineering and Automation, Wuhan University, Wuhan, 430072, China.

d. The Institute of Technological Sciences, Wuhan University, Wuhan, 430072, China.

Corresponding Author

R. Huang - School of Material Science and Engineering, Hanshan Normal University, Chaozhou 521041, China, Email : *rhuang@hstc.edu.cn*

Y. Guo - School of Electrical Engineering and Automation, Wuhan University, Wuhan, 430072, China, Email : yguo@whu.edu.cn

S. Lan - Guangdong Provincial Key Laboratory of Nanophotonic Functional Materials and Devices, School of Information and Optoelectronic Science and Engineering, South China Normal University, Guangzhou 510006, China, Email : *slan@scnu.edu.cn*

Experimental Section

Fabrication of Mn^{2+}-doped Cs_4SnBr_6

In this work, Mn^{2+}-doped Cs_4SnBr_6 were synthesized by water-assisted wet ball-milling. Cesium bromide (4 mmol, CsBr, Aladdin, 99.9%), stannous fluoride (1 mmol, SnF_2, Macklin, 99.9%), ammonium bromide (1 mmol, NH_4Br, Aladdin, 99.99%), and manganous bromide ($MnBr_2$, Macklin, 99%) were used as the reactant precursors. In order to obtain Mn^{2+}-doped Cs_4SnBr_6 with different levels, the molar ratio of CsBr, SnF_2, and NH_4Br were maintained to be 4, 1, and 2 mmol, respectively, whereas the molar ratio of $MnBr_2$ was varied from 0 to 2 mmol. First, the mixture of the precursors was loaded into a jar and mixed with 60 μL deionized water. Then, a ball milling was performed for 60 min at a speed of 600 rpm. After that, the obtained product was dried in a vacuum drying oven for 240 min at a temperature of 60°C. After cooling to room temperature, the Mn^{2+}-doped Cs_4SnBr_6 powder was obtained by ball milling for 60 min at a speed of 600 rpm. Samples with different doping levels were named as S-x, where x = 0, 0.5, 1, and 2 represents the molar ratio of $MnBr_2$.

Characterization of Mn^{2+}-doped Cs_4SnBr_6

The crystal structures of Mn^{2+}-doped Cs_4SnBr_6 were characterized by X-ray diffraction (XRD) (Bruker D8 Advance) at 35 kV and 35 mA. The compositions of Mn^{2+}-doped Cs_4SnBr_6 were analyzed by energy dispersive spectroscopy (EDS) (Bruker EDS QUANTAX). The diffuse reflectance spectra of Mn^{2+}-doped Cs_4SnBr_6 were obtained by using a spectrophotometer (Shimadzu UV-Vis 3600). The PL measurements, including the temperature-dependent PL spectra, and the time-resolved PL spectra, were carried out by using

a PL spectrometer (FLS1000, Edinburgh Instrument). The PLQYs were directly measured by using a PL spectrometer (FLS1000 Edinburgh Instrument) with an integrating sphere and excitation light at 350 nm. In addition, the measured procedure was repeated three times for the spectra of all the samples.

Theoretical calculations based on the density functional theory (DFT)

Theoretical calculations were carried out based on DFT as implemented in the Vienna Ab initio Simulation Package.[1-3] The projector-augmented wave method was employed to calculate the interaction between the ionic cores and valence electrons.[4-5] The Perdew–Burke–Ernzerhof approach of spin-polarized generalized gradient approximation was used to describe the exchange-correlation energy.[6] A larger 2 × 2 × 2 supercell was calculated to characterize the doping effects, which contained 176 atoms. Calculations were performed with the cutoff plane-wave kinetic energy of 520 eV, and 3 × 3 × 1 k-mesh grids were employed for the integration of the Brillouin zone. All atomic positions were fully relaxed until energy and force reached the tolerance of 1×10^{-5} eV and 0.02 eV $Å^{-1}$, respectively. The VASPKIT code was used for postprocessing of the VASP computational data.[7]

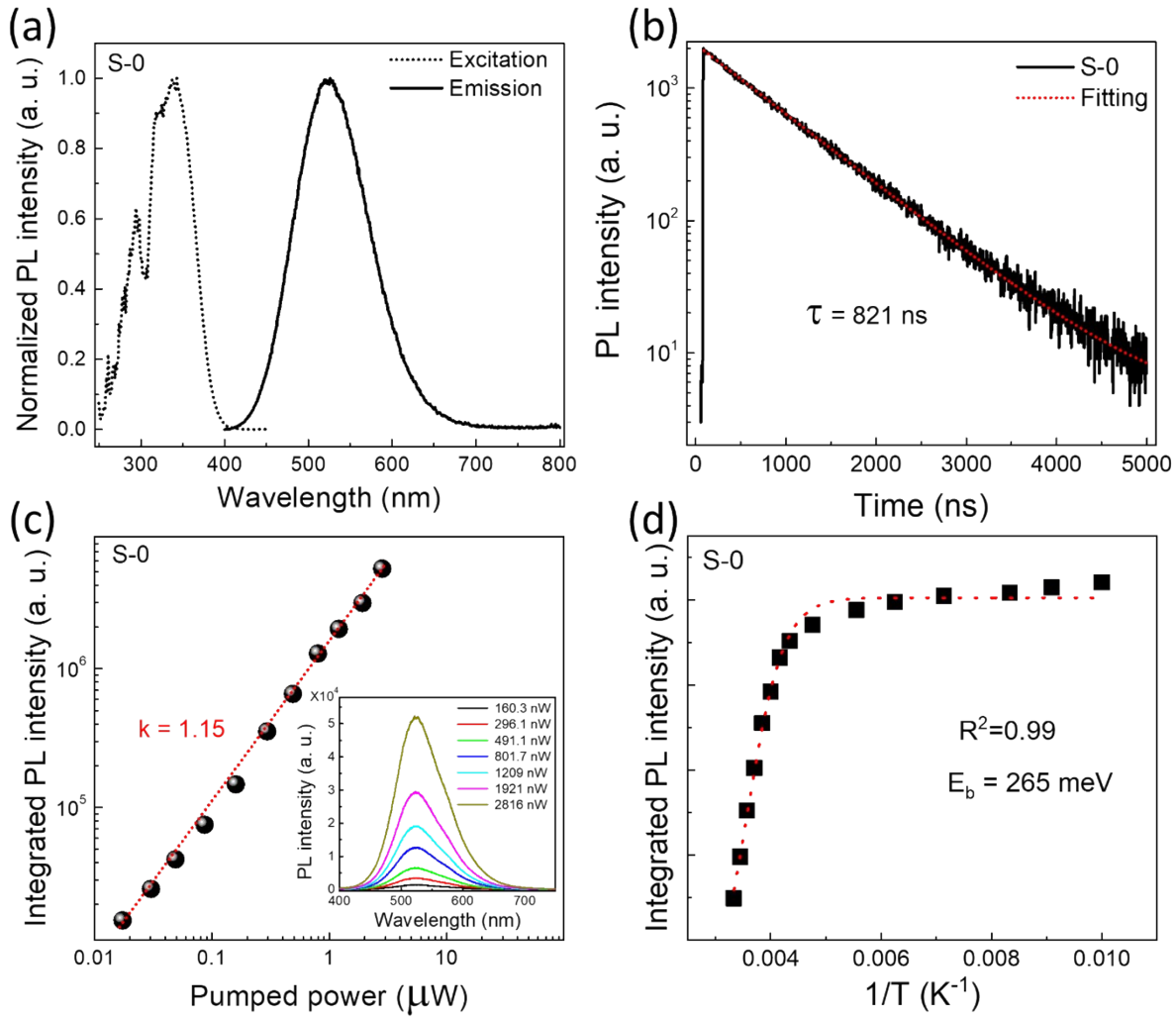

Figure S1 (a) Emission spectrum of sample S-0 and the excitation spectrum recorded at 530 nm. (b) Time-resolved PL decay trace measured for sample S-0. The lifetime was derived by fitting the PL trace with a single exponential decay function. (c) Integrated PL intensity as a function of the excitation power plotted in a logarithmic coordinate for sample S-0. (d) Temperature-dependent PL intensity of measured for sample S-0. The experimental data was fitted by the Arrhenius equation $I_{PL}(T) = \frac{I_{PL}(T_0)}{1 + \beta \exp(-E_b / k_B T)}$, where $I_{PL}(T_0)$ is the integrated PL intensity at 80 K, β is a constant related to the density of radiative recombination centers, k_B is Boltzmann's constant, and E_b is the exciton binding energy.

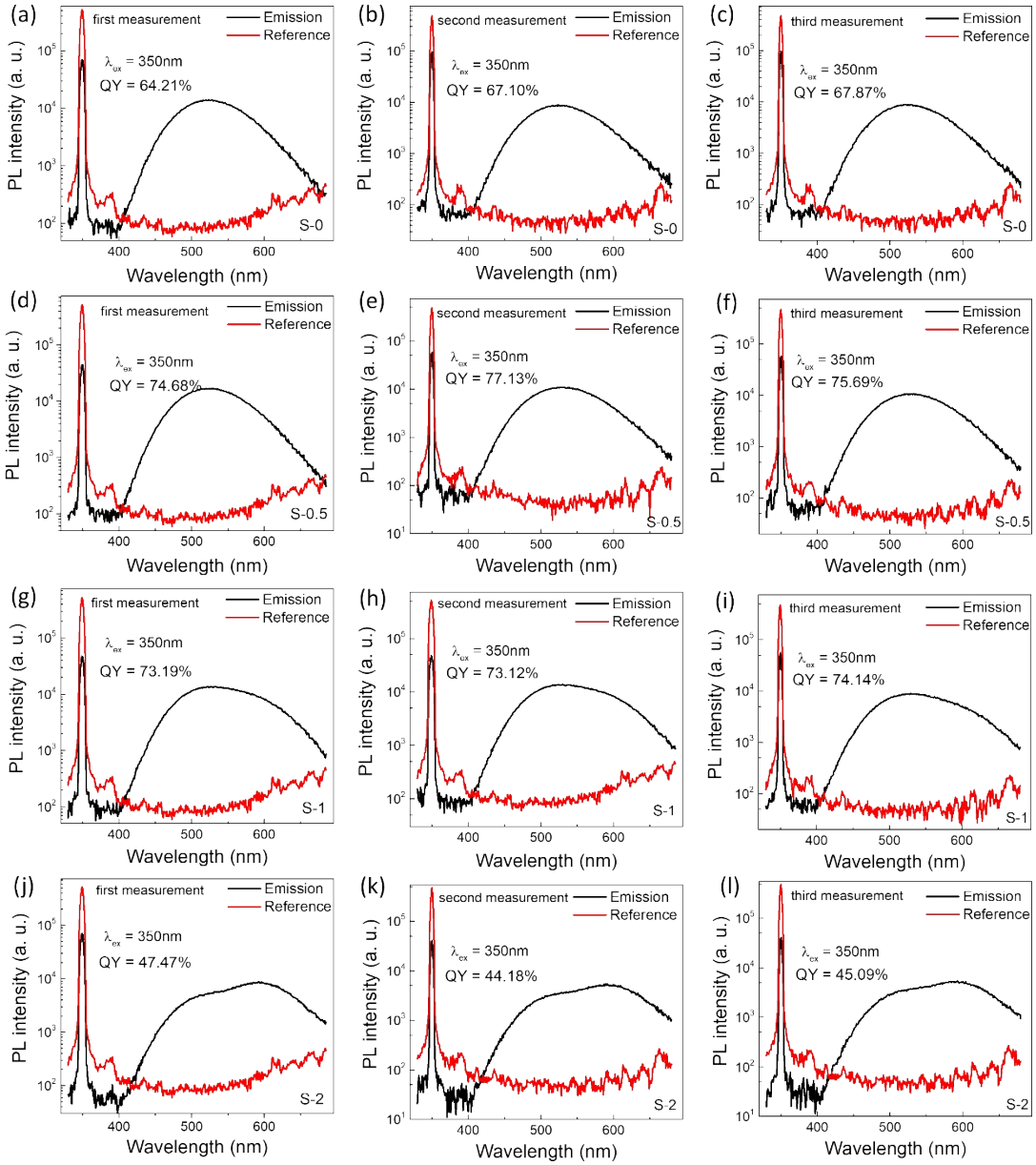

Figure S2 The repeatedly measured excitation and emission spectra measured for the four samples. Excitation spectra measured for all the samples at the peak wavelengths of 350 nm. In each case, the PL QY derived from the excitation and emission spectra is also provided.

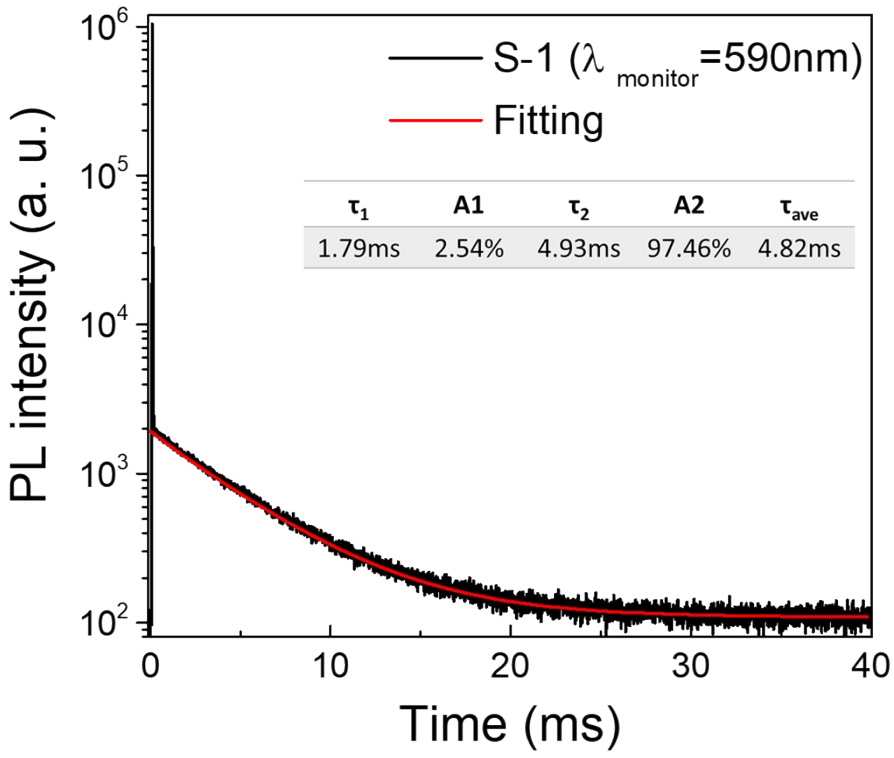

Figure S3 Time-resolved PL decay trace of I_{Mn} recorded at 590 nm for sample S-1. The lifetime was derived by fitting the PL trace with a bi-exponential decay function. The inset shows the fitting result.

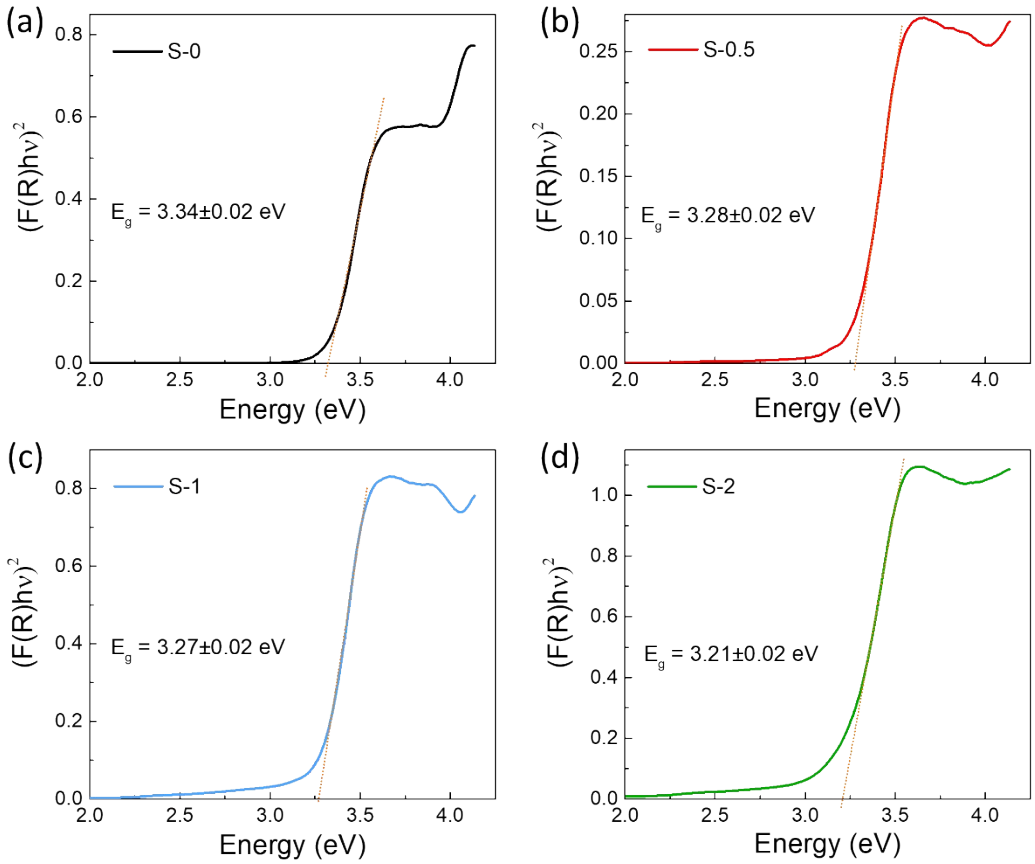

Figure S4 Kubelka-Munk transformed diffuse reflectance spectra of the four samples for determination of the band gap (E_g) by plotting $[F(R)h\nu]^2$ versus hν, where R is the reflectance and F(R) is the Kubelka-Munk function ($F(R) = (1-R)^2/2R$). The values of the band-gap energy can be estimated from the intercepts of the fitted dashed straight lines.

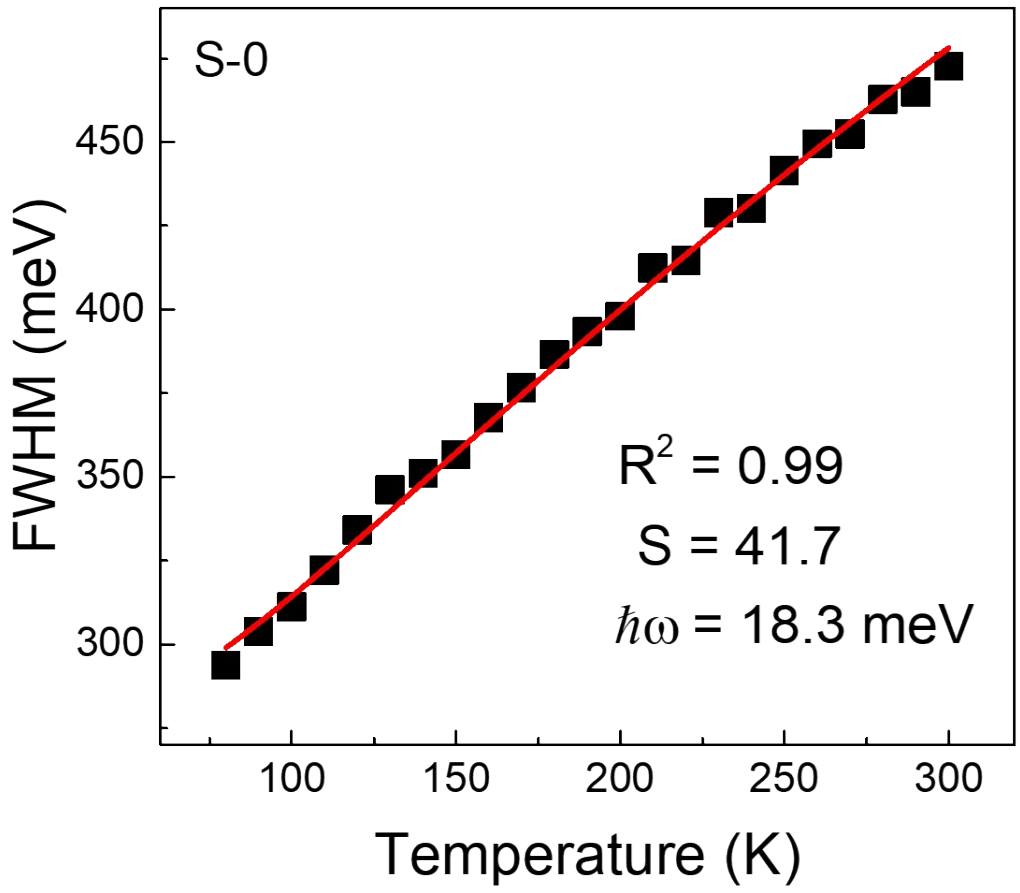

Figure S5 (a) Temperature-dependent linewidth (FWHM) measured for sample S-0, which was fitting by the formular:

$FWHM(\mathrm{T}) = 2.36\sqrt{S}\hbar\omega\sqrt{\coth\frac{\hbar\omega}{2k_BT}}$, where S is the Huang-Rhys factor, $\hbar\omega$ is the energy of the phonon mode, and k_B is Boltzmann's constant.

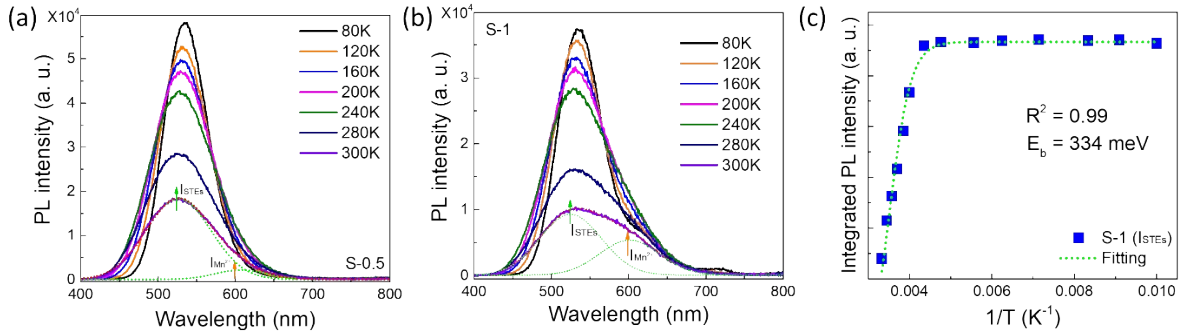

Figure S6 PL spectra measured for sample S-0.5 (a) and S-1 (b) at different temperatures. The dashed line corresponds to deconvolution of PL spectrum measured at 300K. (b) Temperature-dependent PL intensity of I_{Host} based on deconvolution results for sample S-1, which was fitted by the Arrhenius equation $I_{PL}(T) = \frac{I_{PL}(T_0)}{1 + \beta \exp(-E_b / k_B T)}$, where $I_{PL}(T_0)$ is the integrated PL intensity at 80 K, β is a constant related to the density of radiative recombination centers, k_B is Boltzmann's constant, and E_b is the exciton binding energy.

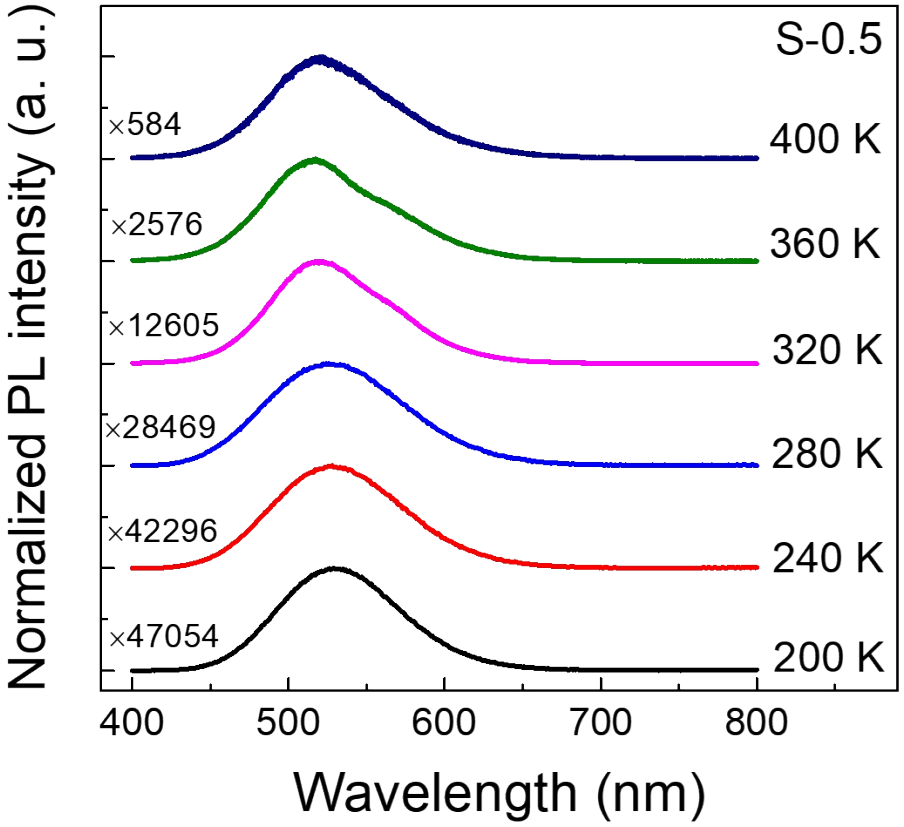

Figure S7 Normalized PL spectra measured for sample S-0.5 at different temperatures.

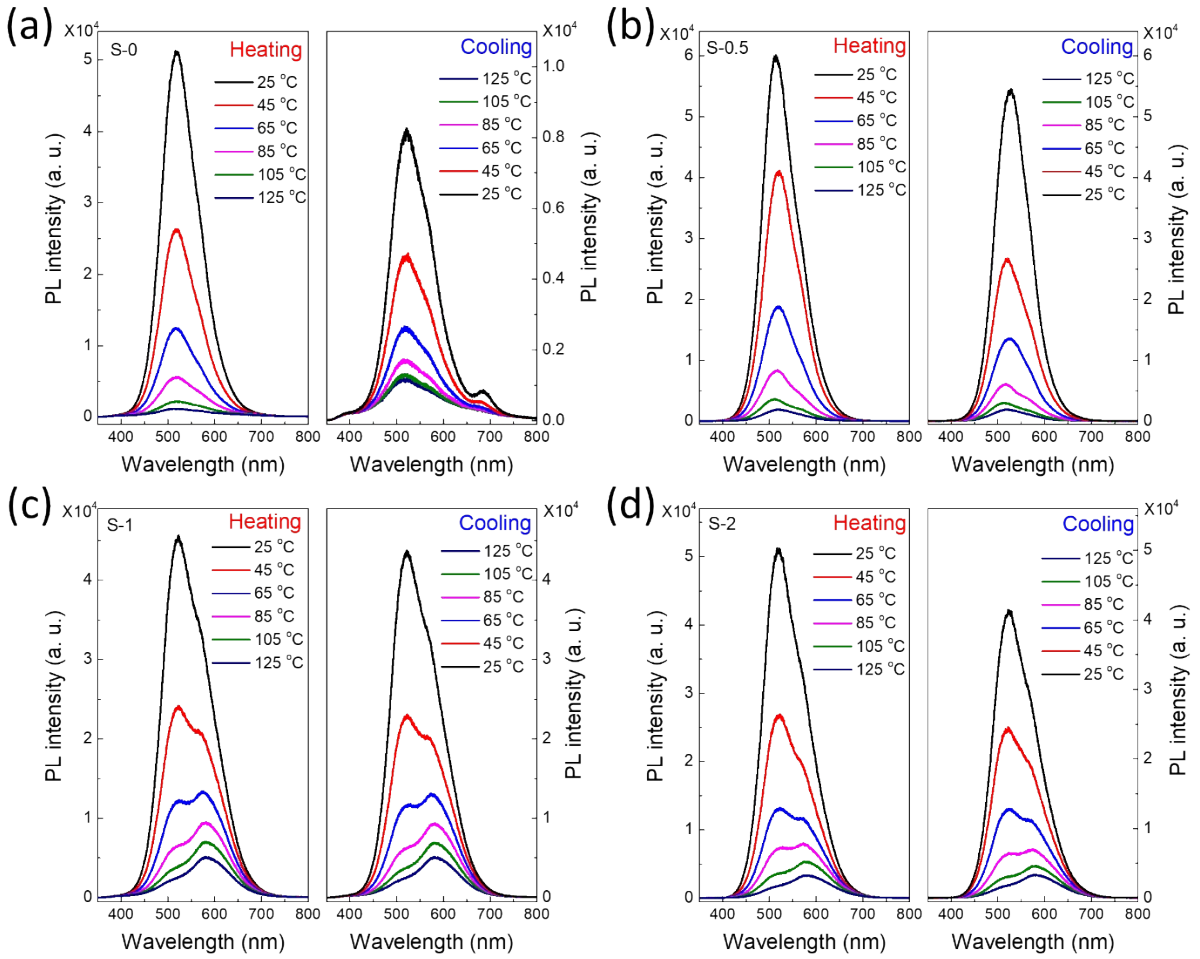

Figure S8 Temperature-dependent PL spectra measured for the four samples in a heating/cooling cycle up to 125℃.

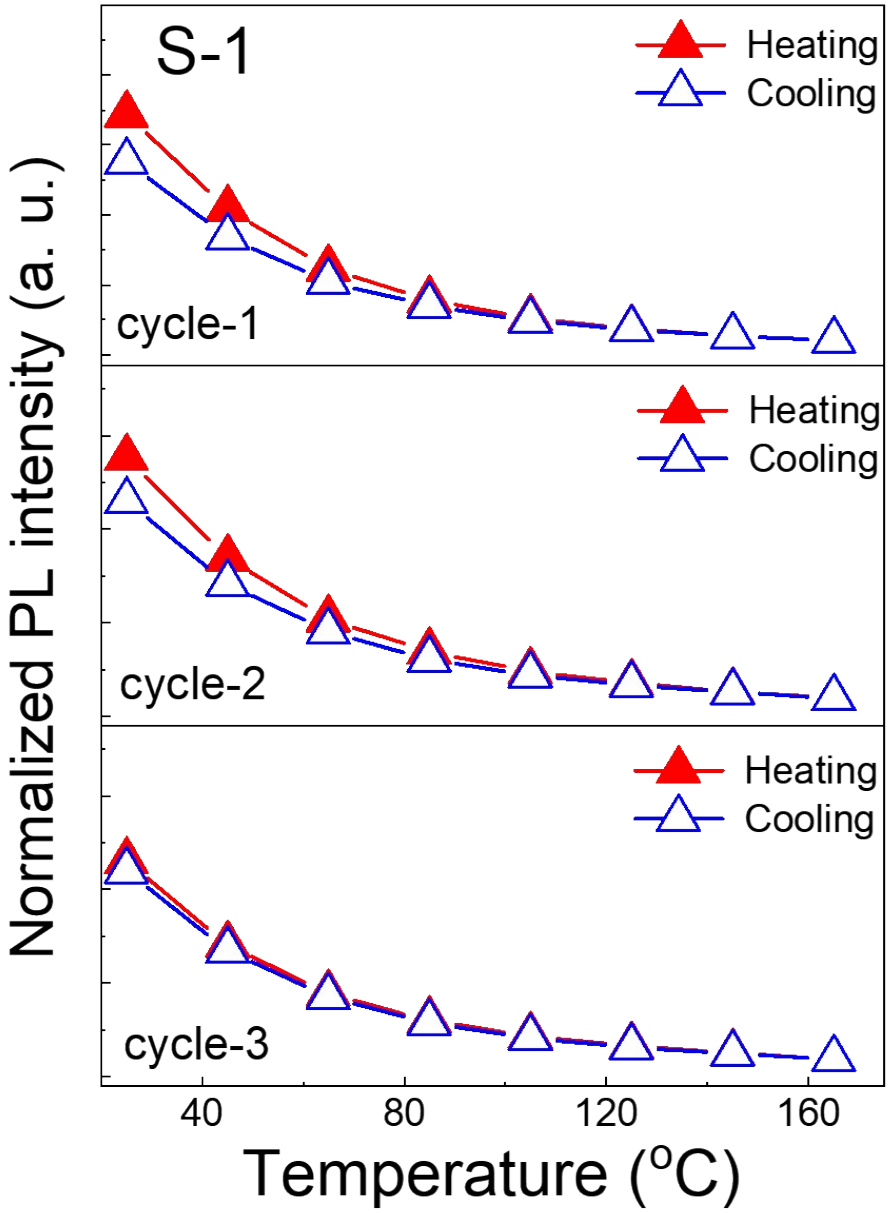

Figure S9 Temperature-dependent PL intensity observed for sample S-1 in three heating/cooling cycles up to 165°C.

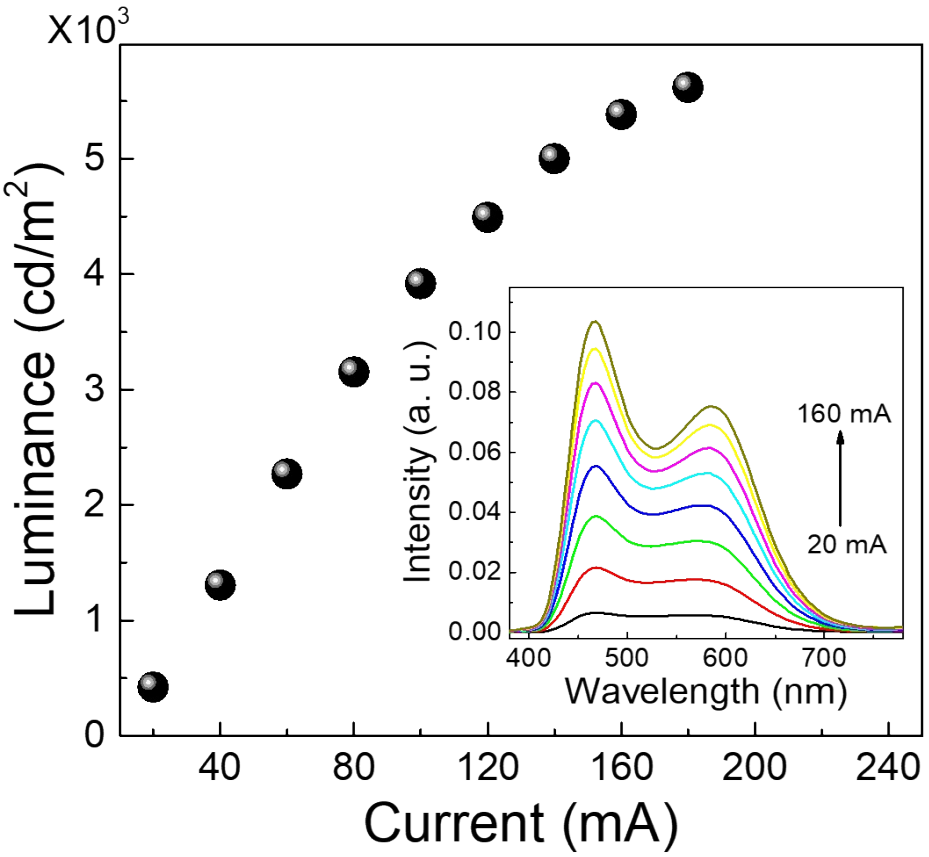

Figure S10 Luminance characteristics of the white LED as a function of the injected current. The inset shows the emission spectra of the LED measured at different injected currents.

Table 1 Survey of the PL QYs of Cs_4SnBr_6 reported in literature.

Year	Materials	QY
2018[8]	Cs_4SnBr_6 powders	15 ± 5%
2019[9]	Cs_3KSnBr_6 microcrystalline	35%
2020[10]	Cs_4SnBr_6 nanocrystalline	21%
2022[11]	Cs_4SnBr_6 nanocrystalline	52%
2022[12]	Cs_4SnBr_6-SnF_2 powders	62.8%
2023 (our work)	Mn^{2+} doped Cs_4SnBr_6 powders	75.8%

Table 2 Comparison of the Cs, Sn, F, Br, and Mn contents in the four samples based on the EDS measurements.

	Cs (%)	Sn (%)	F (%)	Br (%)	Mn (%)
S-0	27.98	9	24.20	38.83	
S-0.5	29.58	7.93	5.62	50.23	6.63
S-1	21.40	7.03	14.91	46.98	9.96
S-2	22.19	4.12	1.48	57.11	15.10

References

(1) G. Kresse, and J. Furthmüller, *Comput. Mater. Sci.,* 1996**, 6,** 15.

(2) G. Kresse, and J. Furthmüller, J. *Phys. Rev. B,* 1996**, 54,** 11169.

(3) G. Kresse, and J. Hafner, *Phys. Rev. B,* 1994, **49,** 14251.

(4) P. Blöchl, *Phys. Rev. B,* 1994, **50,** 17953.

(5) G. Kresse, and D. Joubert, *Phys. Rev. B,* 1999, **59,** 1758.

(6) J. P. Perdew, K. Burke, and M. Ernzerhof, *Phys. Rev. Lett.,* 1996, **77,** 3865.

(7) V. Wang, N. Xu, J. Liu, G. Tang, and W. Geng, *Comput. Phys. Commun.,* 2021, **267,** 108033.

(8) B. M. Benin, D. N. Dirin, V. Morad, M. Wörle, S. Yakunin, G. Rainò, O. Nazarenko, M. Fischer, I. Infante, and M. V. Kovalenko, *Angew. Chem. Int. Ed.,* 2018, **57,** 11329.

(9) X. Zhang, H. Wang, S. Wang, Y. Hu, X. Liu, Z. Shi, V. L. Colvin, S. Wang, W. W. Yu, and Y. Zhang, *Inorg. Chem.,* 2019, **59,** 533.

(10) L. Tan, W. Wang, Q. Li, Z. Luo, C. Zou, M. Tang, L. Zhang, J. He, and Z. Quan, *Chem. Commun.,* 2020, **56,** 387.

(11) K. Xu, Q. Wei, H. Wang, B. Yao, W. Zhou, R. Gao, H. Chen, H. Li, J. Wang, and Z. Ning, *Nanoscale,* 2022, **14,** 2248.

(12) Q. Zhang, S. Liu, M. He, W. Zheng, Q. Wan, M. Liu, X. Liao, W. Zhan, C. Yuan, J. Liu, H. Xie, X. Guo, L. Kong, and L. Li, *Angew. Chem. Int. Ed.,* 2022, **61,** e202205463.